Optical Materials 124 (2022) 112038

Contents lists available at ScienceDirect

Optical Materials

journal homepage: www.elsevier.com/locate/optmat

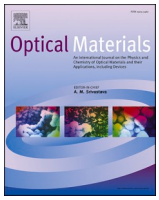

Investigation on phase-modulation characteristics and transmission of the liquid crystal device under continuous-wave laser irradiation

Xiaoshuang Wang [a,b], Kun Wang [a,c], Xiaofeng Liu [a,d,*], Yuan-an Zhao [a,d,e,*], Dawei Li [a,d], Zhaoliang Cao [f], Yuchen Shao [a,d,e], Zenghui Peng [g], Ming Tang [b,h], Jianda Shao [a,d,e,i]

[a] Laboratory of Thin Film Optics, Shanghai Institute of Optics and Fine Mechanics, Shanghai, 201800, China
[b] School of Optical and Electronic Information, Huazhong University of Science and Technology, Wuhan, 430074, China
[c] School of Optical-Electrical and Computer Engineering, University of Shanghai for Science and Technology, Shanghai, 200093, China
[d] Key Laboratory of Materials for High Power Laser, Chinese Academy of Sciences, Shanghai, 201800, China
[e] Center of Materials Science and Optoelectronics Engineering, University of Chinese Academy of Sciences, Beijing, 100049, China
[f] Jiangsu Key Laboratory of Micro and Nano Heat Fluid Flow Technology and Energy Application, School of Physical Science and Technology, Suzhou University of Science and Technology, Suzhou, 215009, China
[g] State Key Laboratory of Applied Optics, Changchun Institute of Optics, Fine Mechanics and Physics, Changchun, 130033, China
[h] Wuhan National Laboratory for Optoelectronics (WNLO) & National Engineering Laboratory for Next Generation Internet Access System, China
[i] Center for Excellence in Ultra-Intense Laser Science, Chinese Academy of Sciences, Shanghai, 201800, China

ARTICLE INFO

Keywords:
Liquid crystal
Laser
Phase modulation
Thermal simulation
Phase simulation

ABSTRACT

Liquid crystal devices (LCDs) are widely used in several applications involving high-power lasers, such as laser processing, laser shaping, laser communication, laser radar and so on. Investigation on the performance of the LCDs working in high-power laser has always been of concern. In this study, a modified nearly common-path interferometry technique is proposed to investigate the phase modulation characteristics of the LCD irradiated by 1064 nm continuous-wave (CW) laser with Gaussian beam profile and an effective area of 0.1 cm^2. In addition, the temperature rise of the LCD induced by laser irradiation was synchronously measured with an infrared thermal imager. A quantitative and dynamic investigation of the relation between the thermal effect caused by the laser and the phase-modulation variation is reported. Experimental results showed that the trend of temperature increase of the LCD was similar to that of phase shift variation. The theoretical phase shift calculated using the temperature-dependent LC refractive index coincided with the experimental results. This indicated that the refractive index change induced by temperature was the main reason for the phase-modulation variation of the LCD under laser irradiation. When the laser power was further increased, interference fringe distortion appeared, and morphological changes in the LC were observed. This implied that the laser-induced temperature rise had reached the clearing point of the LC and that the LCD was inactive. The temperature simulation along the laser incidence direction implied that, under the irradiation CW laser, indium tin oxide (ITO) layer absorbs laser energy, resulting in a temperature rise and a small temperature gradient between the ITO, polyimide (PI) and LC layers. The rising temperature is too low to induced damage of ITO layer and PI layer, but influences the refractive index of the LC. Compared with other layers of the LCD, the LC material will fail first when the irradiated laser power is further risen. The transmission variation of an LCD induced by laser irradiation was found. Possibly owing to the refractive index change of the LC as well as the multilayer film structure of the LCD, there seemed to be a cyclical transmission variation.

1. Introduction

Liquid crystals (LCs), are widely used in display imaging and astronomy fields such as LC displays [1,2], holographic imaging [3–5], hyperspectral imaging [6,7], adaptive optics [8,9], and also in many applications involving high-power lasers such as laser processing [10–12], laser shaping [13,14], laser communication [15] and laser radar [16] owing to their unique elector-optic birefringence properties.

* Corresponding authors. Laboratory of Thin Film Optics, Shanghai Institute of Optics and Fine Mechanics, Shanghai, 201800, China.
E-mail addresses: liuxiaofeng@siom.ac.cn (X. Liu), yazhao@siom.ac.cn (Y.-a. Zhao).

https://doi.org/10.1016/j.optmat.2022.112038
Received 24 November 2021; Received in revised form 12 January 2022; Accepted 21 January 2022
Available online 7 February 2022

Most LCs used in these applications are thermotropic, which means that the LC phase exists within a certain temperature interval (in contrast to lyotropic LC, in which the LC phase exists within a certain concentration range). However, when the high-power laser is projected on the LCD, laser-induced heat inevitably makes the temperature of LCD rise. Performance degradation and likely damage of the LCD are present in these high-power laser applications. So, power handing of the LCDs induces some anxiety. Evaluating the performance of the LCDs under high-power laser irradiation are important for guiding their practical applications in high-power lasers.

Watson et al. studied the phase-modulation characteristic variation of a LCD exposed to a 1083 nm continuous-wave (CW) laser based on the intensity of the probe laser after passing through the analyzer [17]. The results indicated that the phase-modulation characteristic of the LCD with fused silica substrates was not affected when the irradiation laser power was lower than 10 W ($1/e^2$ diameter: 5 mm), and however its phase-modulation depth decreased monotonically as the applied laser power was gradually increased to 80 W. Furthermore, the overall migration of LC molecules was observed after repeated exposure to the CW high-power laser. Cao et al. found that the transmitted intensity of the probe laser after passing through the analyzer dramatically increased when the LCD with fused silica substrates was exposed to an 808 nm laser with a power density higher than 133 W/cm^2, and subsequently remained almost constant when the laser power density was more than 187 W/cm^2 [18]. Zhu et al. reported that the phase response of a LCD with a silicon substrate started to deviate above 80 W ($1/e^2$ diameter: 10 mm) under high average power picosecond laser irradiation, and its temperature measured with an infrared thermal imager increased by only 5 °C at 220 W incident power [19]. Xi et al. proposed the monitoring of the full-filed phase-modulation characteristic of a LCD under 1064 nm high-power laser irradiation by double optical path holographic interferometry [20]. The hologram recorded after the LCD was irradiated changed with the laser irradiation power and time. The temperature increase of the LCD was also captured by the thermocouple, which can directly contact the LCD except for the area of the laser irradiation. However, the temperature results did not agree with the dynamic process of phase change induced by laser irradiation, and continued to increase after shutting down the high-power laser. This occurred because the position where thermocouple was located was far away from the irradiated area. Therefore, the detected temperature was not synchronized with the actual temperature rise of the LCD. Moreover, when a laser beam propagates through the LCD, spatial self-phase modulation may be generated, thus a multiple-ring pattern can be observed in the far-filed. The phase modulation variation of the LCD induced by laser irradiation can be estimated by $\varphi = N \times 2\pi$, in which N is the number of the ring [21,22].

In terms of theoretical simulation, to optimize the working conditions of the LCD on the incident laser power, the influences of absorption, the heat sink structure, the cooling fluid rate, and the substrate on the laser-induced phase distortion of the LCD were calculated based on the heat deposition and heat transfer model [23,24]. When the incident laser power was 110 W and the total indium tin oxide (ITO) absorption was 5%, a heat sink structure with a flow rate of 0.01 m/s caused laser-induced phase deformation at the center of the LCD to be less than 0.06, and the maximum temperature increase at the center was less than 1 K [25]. This information is critical for improving the powering handling limitations of LCDs.

Existing studies have not experimentally investigated the relationship between the actual dynamic thermal response and the phase-modulation variation of the LCDs working in the high-power laser [17–25]. In addition, in the transmission change of the LCD induced by laser irradiation, the phase-modulation characteristics obtained based on the intensity analysis of the probe laser after passing through the analyzer are unreliable [17,18]. Laser-induced multiple rings can be generated only for the LCD with thick LC layer or dye-doped LC [21,22]. Double optical path holographic interferometry is sensitive to external environmental vibrations and temperature changes [20]. In this study, a modified nearly common-path interferometry is proposed to investigate the phase-modulation characteristics of an LCD with a thin LC layer under a 1064 nm CW laser with a Gaussian beam profile and an effective area of 0.1 cm^2. In addition, the temperature rise of the LCD induced by laser irradiation was synchronously measured with an infrared thermal imager. We analyzed the phase-modulation variation and thermal response, and then established the relationship between the LCD phase-modulation variation and temperature. In order to clarify the deposition of laser energy in the LCD, the temperature distribution in the LCD was simulated. Experimental results showed that the trend of temperature increase of the LCD was similar to that of phase shift variation. When the laser power was further increased, the uniform phase-modulation behavior vanishes, and visible morphological changes can be observed by the on-line CCD. However, uniform phase-modulation behavior can be restored once the laser is removed or the power decreases. The temperature simulation along the laser incidence direction implied that, under the irradiation CW laser, indium tin oxide (ITO) layer absorbs laser energy, resulting in a temperature rise and a small temperature gradient between the ITO, polyimide (PI) and LC layers. The rising temperature is too low to induced damage of ITO layer and PI layer, and however influences the refractive index of the LC. Compared with other layers comprised the LCD, the LC material will fail first when the irradiated laser power is further risen. The transmission variation of an LCD induced by laser irradiation was first reported. Possibly owing to the refractive index change of the LC as well as the multilayer film structure of the LCD, there seemed to be a cyclical transmission variation. This study aims to expand the understanding of the influence of thermal response on the performance of LCDs, and provides guidance on the fabrication and applications of LCDs.

2. Sample preparation and experimental set-up

2.1. Sample preparation

The LCD consists of a number of thin layers sandwiched between two K9 glass substrates as shown in Fig. 1. ITO transparent conductive films were coated onto the inside surfaces of the glass. The PI alignment layer, which determines the initial orientation of the LC molecules, was deposited on the ITO films. The LC layer was between two alignment layers, and its thickness was defined by the spacers. The specific parameters of the samples are listed in Table 1. The thickness of the thin LC layer is 7 μm. The LC material used in our study was positive E7, which was composed of the following monomers: 5CB (51%), 7CB (25%), 80 CB (16%), and 5CT (8%). Compared to a single component of 5CB which clear point only 35 °C, the E7 has higher temperature stability for our experiments [26,27]. Its theoretical clearing point is approximately 59 °C [28], which is estimated by [29].

$$T_{(N-I)} = \sum_{i=1}^{n} X_i \cdot T_{(N-I)i} \tag{1}$$

where $T_{(N-I)i}$ and X_i are the clearing point and mole fraction of each monomer, respectively.

2.2. Experimental setup

2.2.1. Nearly common-path interferometric technique for phase measurement

Double-path interferometry is widely used in phase measurements, as each path can be easily adjusted individually; however, it requires high environmental stability. An improved nearly common-path interferometric technique, as shown in Fig. 2(a), overcoming the above shortcoming, is proposed to measure the phase change of the LCD induced by laser irradiation in our experiment.

A He–Ne laser with a Gaussian beam profile is used as the probe

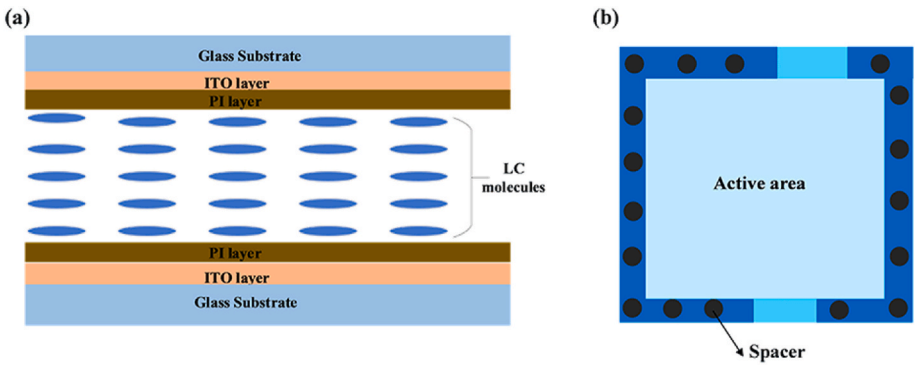

Fig. 1. Structure of the LCD. (a) Sectional view. (b) Top view.

Table 1
Primary parameters of each layer of the LCD.

LC material	Glass substrate	ITO layer	PI layer	LC layer	Clearing point	Birefringence
Positive E7	1 mm	100 nm	80 nm	8 μm	59 °C	$\Delta n = 0.21, n_e = 1.73, n_o = 1.52$ (632.8 nm, 25 °C)

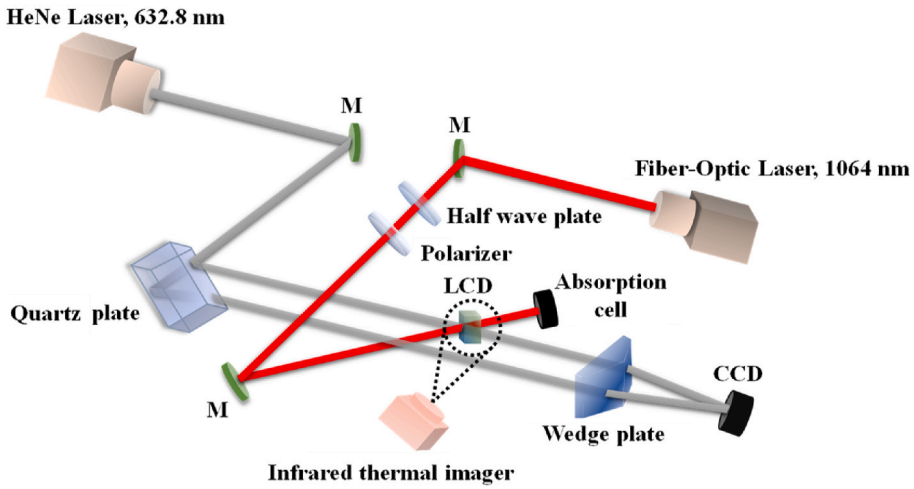

Fig. 2. Schematic diagram illustrating the nearly common-path set up.

beam to form interference pattern. It is split into two beams via the front and back surfaces of the 1 cm thick fused quartz, and these beams act as the object and reference beams. The object beam passing through the LCD is combined with the reference beam via the isosceles triangular wedge. Compared with the focusing lens, the isosceles triangular wedge plate makes the size of the interferogram more appropriate. In this setup, the object beam shares approximately the same optical path as the reference beam. Therefore, the measurements are insensitive to experimental environmental effects, such as vibration and airflow. This contributes to stable interferograms and ensures the accuracy of the measurement results. The 1064 nm CW laser beam with a Gaussian beam profile, as a pump laser, passes through the attenuation system consisting of a half-wave plate and polarizer and then irradiates directly on the LCD. The polarization of the pump is parallel to the long axis of the LC molecule. The center of the pump beam is coincident with the center of object beam on the LCD. The effective area of the object beam on the LCD incidence surface is 0.97 mm^2, whereas it is 0.1 cm^2 for the pump laser at the normal incidence. Hence, the phase measurement results can be considered as a single point measurement (the point located in the center of the pump laser facula), and the phase variation in the interferogram should be uniform and consistent.

The infrared thermal imager recorded the actual temperature of the LCD in real time. The emissivity parameter of the LCD was proved to be similar to that of a fused silica substrate [30,31]. The parameters used in the infrared thermal imager are listed in Table 2. The infrared thermal image gives the maximum temperature rise of the LCD, just representing the temperature of the point located in the center of the pump laser facula. The measured temperature was almost unchanged when the infrared thermal imager was located 40 cm–100 cm away from the LCD in our experiment. Moreover, an on-line CCD was used to observe the morphology of the LCD under laser irradiation.

The stability of the setup was verified without pump laser irradiation. The measured interferogram and intensity distribution of interference fringes without irradiation are shown in Fig. 3. Fig. 3(a) shows one of the interferograms. Fig. 3(b) shows the intensity distribution of the interference fringes along the red line extracted from six interferograms measured at 0, 2, 4, 6, 8, and 10 min. It should be pointed out that

Table 2
Infrared thermal imager measurement parameters.

Model	Emissivity	Atmospheric temperature	Atmospheric humidity	Distance
A615	0.93	25 °C	0.35	70 cm

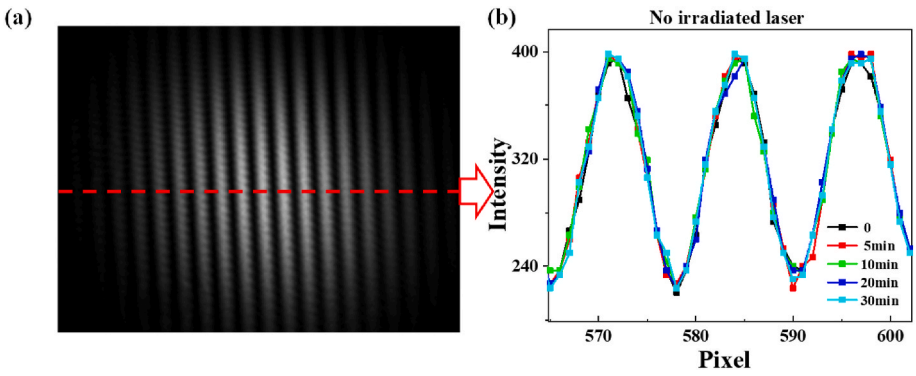

Fig. 3. (a)Interferogram obtained by the CCD. (b) Intensity distribution along the red line in (a).

the intensity distributions of the interference fringes given in our study are all along the red line illustrated by Fig. 3(a). As can be seen from Fig. 3(b), the fringes almost did not move within 10 min. This proves the stability of our nearly common-path setup, which is very important for the accuracy of the phase measurement.

The interference fringes formed by the reference and object beams will shift if the phase modulation characteristics of the LCD are changed. The phase modulation can be calculated using the shift of the intensity distribution of the interference fringes, which can be expressed as [32]:

$$\Delta\varphi = 2\pi(\Delta / \Lambda) \tag{2}$$

where Δ and Λ are the horizontal movement distance and period of the fringes, respectively, and the units of both are the number of pixels.

In addition to the phase, transmittance is another important parameter for LCD applications. Therefore, we adjusted the setup and explored the probe laser to measure the transmittance change under pump laser irradiation. Quartz plate was removed and replaced by mirrors. The probe laser passing through the LCD does not have to be focused again. The probe laser passing through the irritated area of the LCD by the pump laser. The center of the pump beam on the LCD is coincident with the center of probe beam on the LCD. The intensity of the probe beam after irradiation on the LCD was directly recorded by a power meter.

Here the transmission variation rate of the LCD is defined as:

$$\Delta T = \frac{I_i - I_0}{I_0} \times 100\% \tag{3}$$

where I_i and I_0 are the intensities of the probe laser with and without pump laser loading, respectively.

3. Results

3.1. Effect of laser irradiation on phase modulation characteristics of the LCD

The interference fringes formed by the reference and object beams shift if the phase modulation characteristics of the LCD are changed. Fig. 4 shows the intensity distribution of the interference fringes under 400 mW laser irradiation. The period of the fringes was approximately 12 pixels. The interference fringes shifted left as the irradiation time was increased, as shown in Fig. 4(a), and no evident changes in morphology can be observed in Fig. 4(b).

In our study, the phase-modulation variation of the LCD under an irradiated laser from 100 mW to 1900 mW within 300 s was investigated. As shown in Fig. 5(a), the phase shift of the object beam produced by the LCD maintained the original condition when the irradiated laser power was lower than 100 mW and started to change when the irradiated laser power was increased to 200 mW. When the laser power was increased from 200 to 1500 mW, the phase shift of the object beam rapidly increased within ~60 s and then gradually tended to a stable value. The final phase shift of the object beam produced by the LCD increased from 0.17 π to 1.5 π as the irradiated laser power increased from 200 to 1500 mW. The temperature of the laser irradiation region measured by the infrared thermal imager is shown in Fig. 5(b). The temperature induced by different irradiated laser powers rapidly increased within ~60 s and subsequently tended to stabilize, which behaved similarly with the phase shift increase. The maximum temperature of the LCD induced by the 200 mW laser power irradiation was ~28.3 °C and increased monotonically as the irradiated laser power increased. The maximum temperature induced by the laser power of 1500 mW was ~48 °C, which did not reach the clearing point of the LC.

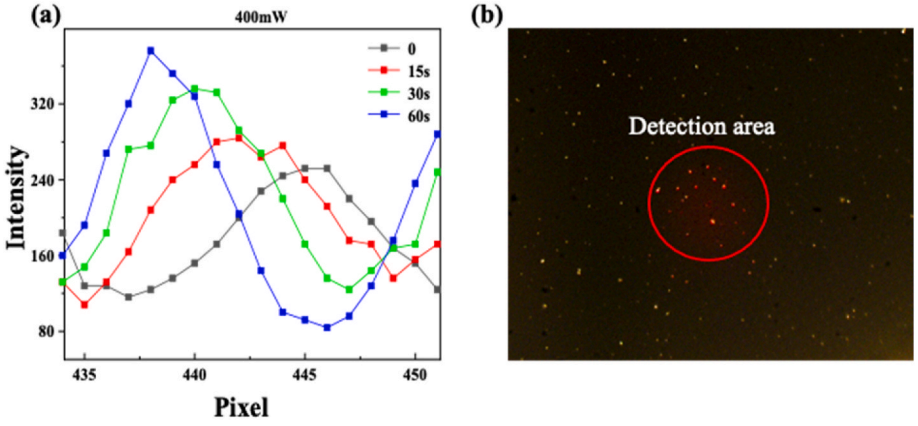

Fig. 4. (a) Variation of the intensity distribution of interference fringes with increasing time when the irradiation laser power is 400 mW. (b) Morphology of the LCD after laser irradiation of 60 s.

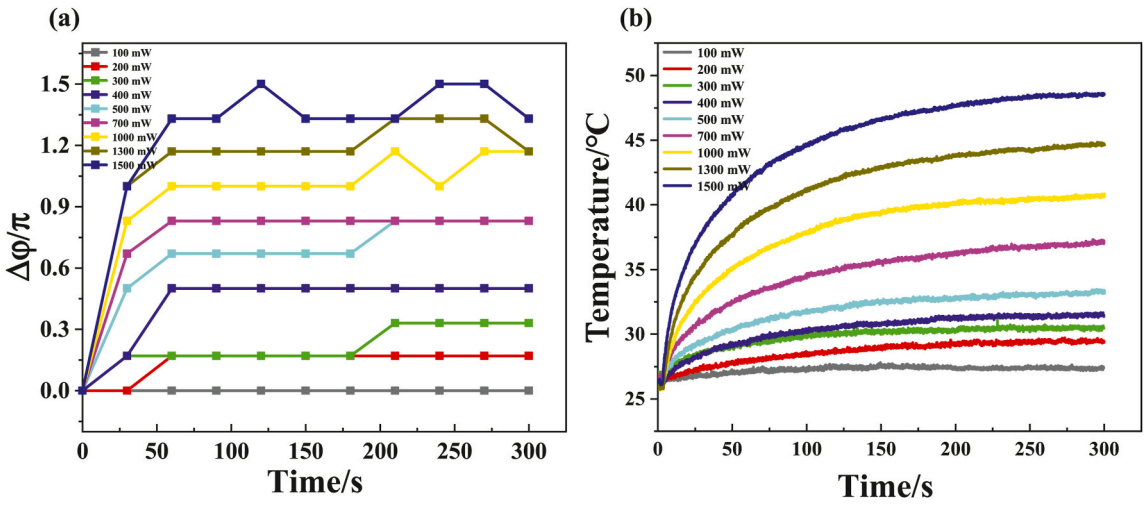

Fig. 5. (a) Variation of phase modulation of LCD with time under different irradiation laser power. (b) Variation of temperature of LCD versus time under different irradiation laser power.

When the irradiated laser power increased to 1700 mW, the interference fringe distortion occurred, as shown in Fig. 6(a) and (b), and the phase shift value could not be extracted, indicating non-ununiform phase-modulation variation. In addition, visible morphological changes could be observed, as shown in Fig. 6(c), and the temperature of the LCD reached 52.5 °C as shown in Fig. 6(d), close to the clearing point of the LC. Considering the error of the measured temperature, the morphological change of the LC implied that the temperature rise induced by the pump laser irradiation had reached the clearing point of the LC. At the clearing point temperature, the LC phase started to convert to an isotropic liquid. So, the uniform phase-modulation behavior vanished and the LCD becomes inactive.

The morphological changes were more evident under the 1900 mW irradiated laser, as shown in Fig. 7. The white spot in the laser irradiation region expanded even more with the increasing laser irradiation time and gradually stabilized at a certain diameter. Furthermore, the interference fringe intensity distributions before laser turning on and after laser turning off coincided, as shown in Fig. 8. Consequently, the phase-modulation ability can be restored once the laser is removed or the power decreases.

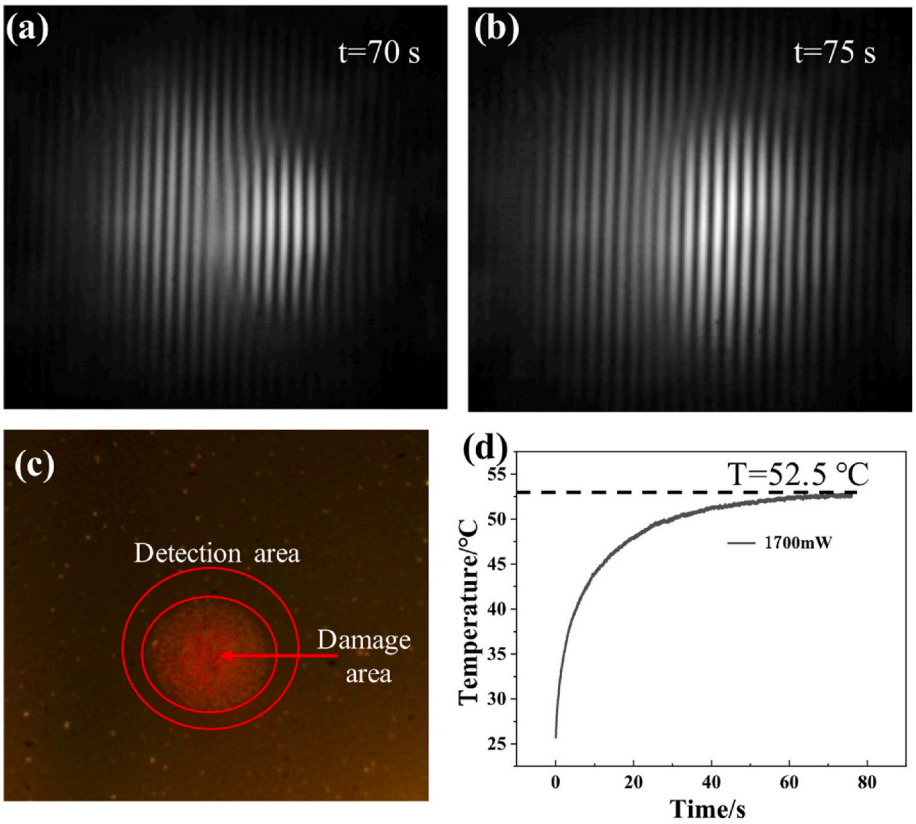

Fig. 6. Interference fringes at 1700 mW power of irradiated laser. (a) Irradiation time of 40 s. (b) Irradiation time of 45 s. (c) LCD morphology. (d) Temperature variation in the laser irradiation region of LCD.

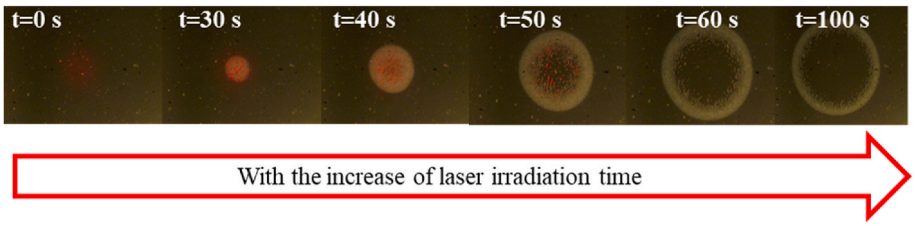

Fig. 7. Morphologies of LCD changes with time under 1900 mW irradiated laser.

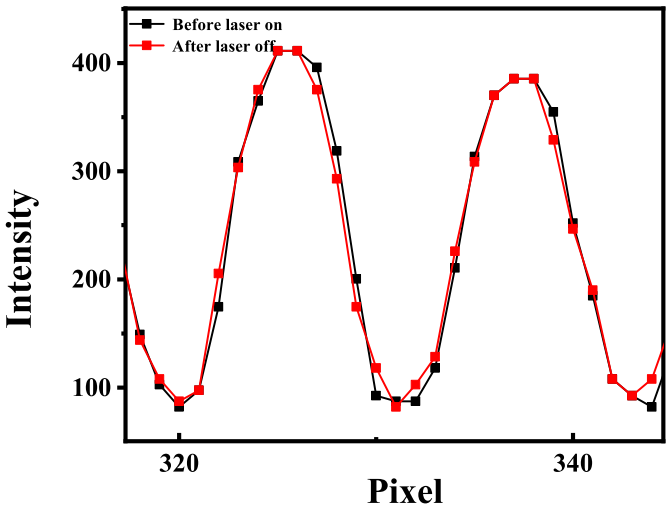

Fig. 8. Intensity distribution of interference fringes before laser turn on and after laser turn off.

3.2. Transmission variation of the LCD induced by laser irradiation

This is the first study to investigate the transmission variation of LCDs during laser irradiation, as shown in Fig. 9. No diffraction rings were observed for the probe laser beam through the irradiated area of the LCD. In Fig. 9(a), there was a short and inconspicuous increase in the transmission of the LCD, followed by a rapid decline to −5% with the irradiation time. However, when the laser power was increased to 800 mW, the transmission decreased first and then increased. In Fig. 9(b), the initial transmission rise was evident within 1200–1500 mW laser irradiation, reaching ~10% as the irradiation time increased. There seems to be a cyclical increase and decrease in the transmission process, as shown in Fig. 9(b).

4. Discussion

The similar tendencies exhibited by the phase shift variation and temperature rise shown in Fig. 6 proves that temperature is an important influencing factor for the phase modulation characteristics of the LCD. The phase shift variation produced by the LCD can be expressed as:

$$\Delta\varphi = \frac{2\pi}{\lambda}\Delta nd \tag{4}$$

where λ is the wavelength of the incident beam, Δn is the birefringence of the LC material and d is the thickness of the LC layer. For the LCD used at a specific laser wavelength, the phase modulation is determined by Δn and d.

It is widely accepted that LC birefringence is sensitive to temperature. The influence of temperature on refractive indices of LC materials was simulated and verified experimentally by S.T. Wu et al. [33,34]. Based this, we further explored the relation between the final phase-modulation variation of the LCD and temperature rise induce by laser loading. The LC birefringence can be expressed by

$$\Delta n = n_e - n_o \tag{5}$$

where n_o and n_e are the ordinary and extraordinary refractive indices, respectively. The following four-parameter model based on the Vuks and Haller equations can describe the temperature-dependent LC indices [34]:

$$\begin{cases} n_e(T) = A - BT + \frac{2}{3}(\Delta n)_0\left(1 - \frac{T}{T_c}\right)^{\beta} \\ n_o(T) = A - BT - \frac{1}{3}(\Delta n)_0\left(1 - \frac{T}{T_c}\right)^{\beta} \end{cases} \tag{6}$$

Parameters A and B can be obtained by fitting the temperature-dependent data at a given wavelength, $(\Delta n)_0$ is the birefringence of an LC in its crystalline state or at T = 0 K, T_c is the clearing point of the LC, and $\beta = 0.20–0.25$ is the material constant that is not sensitive to the LC structure [34]. Subtracting the two equations results in Eq. (6):

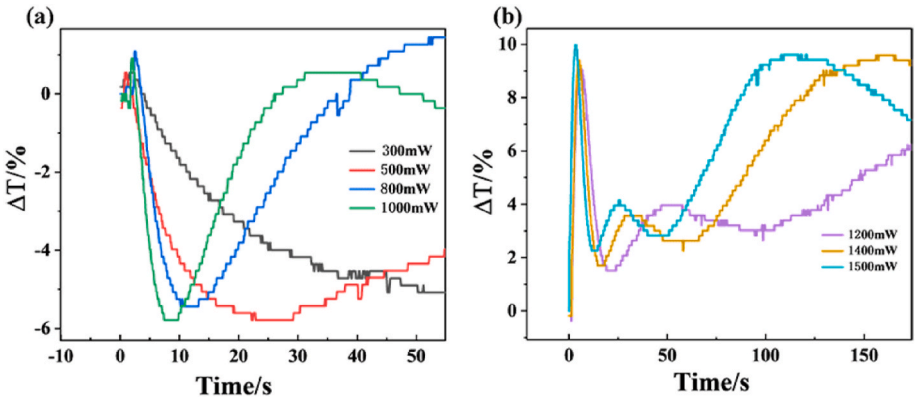

Fig. 9. Curves of transmission variation. (a) Irradiated laser power of 300–1000 mW. (b) Irradiated laser power of 1200–1500 mW.

$$\Delta n(T) = n_e(T) - n_o(T) = (\Delta n)_0(1 - \frac{T}{T_c})^{\beta} \quad (7)$$

where $\Delta n(T)$ is the birefringence of the LC material at a certain temperature that does not exceed the clearing point. The LC layer thickness can be considered unaffected by temperature because lower temperatures are accompanied by less thermal expansion. Therefore, the phase modulation variation caused by the LCD can be estimated by:

$$\Delta\varphi = \frac{2\pi}{\lambda}(\Delta n)_0(1 - \frac{T}{T_c})^{\beta} d \quad (8)$$

The theoretical phase-modulation variations calculated by Eq. (9) compared with the experimental results are shown in Fig. 10. The experimental result was similar to the theoretical phase shift tendency, and both increased with the increase in temperature before the temperature reached the clearing point of the LC. This proves that the temperature-induced refractive index change is the main factor for the LCD phase shift change during laser irradiation. However, the simulation results started to deviate from the experimental data when the temperature was close to the clearing point. This should be related to the LC material degradation, which causes the dependence of the refractive index and temperature to deviate from Eq. (8).

When the LCD working under the high-power laser, the ITO layer absorbed laser energy first because the large absorption coefficient of the ITO. The heat induced by CW laser irradiation in the ITO layer has enough time to conduct to the LC layer, resulting in the temperature rise of the LC. We simulated the thermal temperature distribution of the LCD along the laser incidence direction based on the heat transport model described in Refs. [35–37]. The thermophysical parameters used in our simulation is shown in Table 3.

The geometrical model of the LCD as well as laser incidence direction in the temperature simulation are shown in Fig. 11(a). The thickness of each LCD layer was consistent with Table 1. The Z-axis coordinates help us located the position of each layer comprised the LCD. The laser parameters used in the simulation were consistent with those used in the experiment, which is a 1064 nm CW laser at normal incidence with spot effective area 0.1 cm^2. Three-dimensional temperature distribution induced by 1000 mW laser irradiated within 300 s as shown in Fig. 11 (b). It seems that the two glass substrates absorb little laser energy and most of the heat concentrated in other middle layers of the LCD. The temperature distribution of the irradiated center along the Z-axis are extracted as shown in Fig. 11(c). The temperature distribution along the

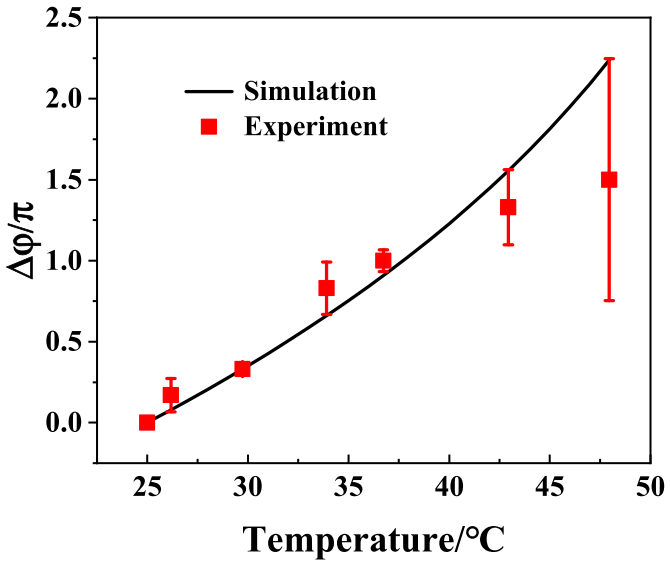

Fig. 10. Comparison of theoretical and experimental values of phase modulation.

Table 3
The thermo-physical parameters of materials in LCD.

Parameter	K9	ITO	PI	LC
Absorption coefficient (m^{-1})	1	5×10^5	1.9	10
Heat transfer coefficient ($W \cdot m^{-1} \cdot °C^{-1}$)	1.4	3.3	0.28	0.5
Specific heat (J•Kg•K)	840	340	814	1765

Z-axis is symmetrically as same as the LCD multilayers structure. The maximum temperature in the LCD is close to ~40 °C, which is nearly coincide with the measured value marked by the yellow line shown in Fig. 5(b). The local magnified view marked by the red rectangle shown in Fig. 11(b) is given in Fig. 11(d). But the temperature of center is not a perfectly symmetrical case as shown in Fig. 11 (d). This is because of the absorption and reflection loss of laser in LCD layers. The ITO layer on the side which laser incident absorbs more energy than the ITO layer on the other. It implies that, under the irritation CW laser, ITO layer absorbs laser energy, resulting in a temperature rise and a small temperature gradient between the ITO, PI and LC layers. This result is different from the behavior of the LCD under pulsed laser irradiation. Under pulsed laser irradiation, the temperature rises rapidly to more than a thousand degree at very short time because of the instant strong absorption in ITO layer and ITO layer damage first [38,39]. Under CW laser irradiation, the rising temperature is too low to induced damage of ITO layer and PI layer, but influences the refractive index of the LC. Compared with other layers, the LC has a low clearing point and undergoes the Nematic-Isotropic phase transition first as the temperature is further risen.

In addition, a cyclical increase and decrease in the transmission should be mainly determined by the refractive index of the LC. The LCD is a multilayer symmetrical film structure composed of a substrate, ITO, an PI layer and an LC layer. The transmission variation of the multilayer structure with different LC average refractive index could be evaluated roughly by TFCals software, which is a commercial software to calculate the multilayer films. The refractive index variation of the LC material depends on the temperature rise induced by laser loading. The average refractive index of the LC material can be expressed as:

$$\langle n \rangle = A - BT \quad (9)$$

where A and B is a fixed parameter of LC material. For E7 material, A = 1.7061, B = 5.75×10^{-4} (/K) when the laser incident at 633 nm. The average refractive index value corresponding to different temperatures could be calculated. The influence of the temperature on transmittance variation at 633 nm could be finally obtained from TFCals. The comparison of experimental and theoretical transmission variation with temperature increase are shown in Fig. 12. It can be seen that the simulation value and experimental value of transmittance variation exhibited some similar characteristics in change trend. Thus, the cyclical increase and decrease transmission variation should be mainly determined by the refractive index of the LC. Each LC refractive index corresponds to a new film system and may result in a cyclical transmission variation of the LCD to some extent.

5. Conclusions

In brief, a nearly common-path interferometry technique that is insensitive to external environment vibrations and temperature changes is first proposed to investigate the LCD phase-modulation characteristics under CW laser irradiation. A quantitative and dynamic investigation of the relation between the thermal effect caused by the laser and the phase-modulation change was reported. The phase shift of the object beam maintained its original condition when the irradiated laser power was lower than 100 mW. When the laser power was increased from 200 to 1500 mW, the phase shift gradually increased from 0.17 π to 1.5π. The phase shift rapidly increased within ~60 s and then gradually stabilized. In addition, the trend of temperature increase of the LCD was similar to

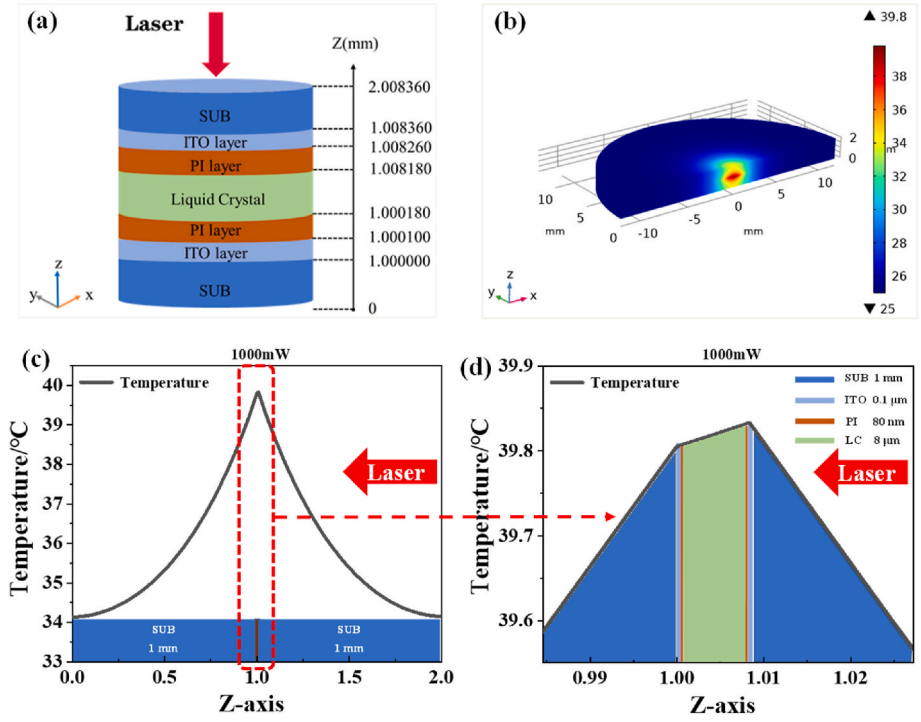

Fig. 11. (a) Geometrical of the LCD used for temperature simulation. (b) Three-dimensional temperature distribution of LCD irradiated by 1000 mW laser for 300 s. (c) The temperature varies with the direction of the z-axis. (d) Amplification of peak location in (c).

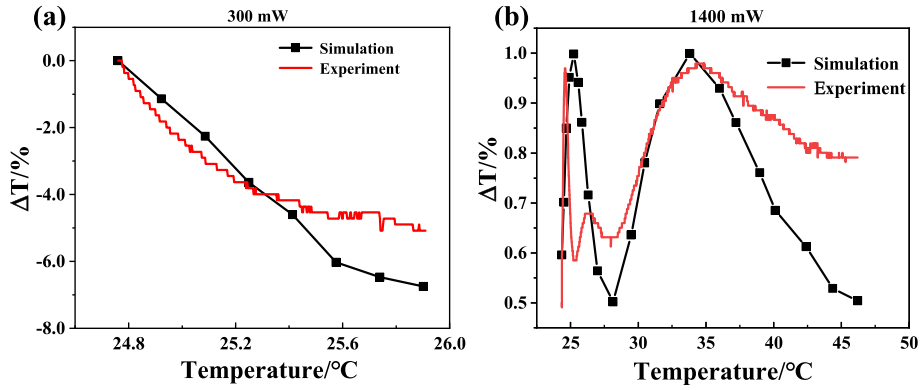

Fig. 12. The simulation and experimental comparison of the transmission variation. (a) Irradiated laser power of 300 mW. (b) Irradiated laser power of 1400 mW.

that of phase shift variation. The theoretical phase shift calculated using the temperature-dependent LC refractive index coincided with the experimental results. This proved that the refractive index change induced by temperature was the main reason for the phase shift change of the LCD under laser irradiation. When the laser power was further increased, interference fringe distortion appeared, and morphological changes of the LC were observed. This implied that the laser-induced heat had reached the clearing point of the LC and that the LCD was inactive. The temperature simulation along the laser incidence direction implied that, under the irradiation CW laser, ITO layer absorbs laser energy, resulting in a temperature rise and a small temperature gradient between the ITO, PI and LC layers. The rising temperature is too low to induced damage of ITO layer and PI layer, but influences the refractive index of the LC. Compared with other layer of the LCD, the LC material will fail first when the irradiated laser power is further risen. The transmission variation of an LCD induced by laser irradiation was first reported. Transmission variation simulation based on the refractive index change of the LC as well as the multilayer film structure of the LCD and experimental results exhibited some similar characteristics in change trend.

Funding

This research was supported by the National Natural Science Foundation of China (Grant No. 11874369 and U1831211); the Open Research Fund of State Key Laboratory of Pulsed Power Laser Technology, China; the Strategic Priority Research Program of the Chinese Academy of Sciences, China (Grant No. XDB1603).

Data availability

Data underlying the results presented in this paper are not publicly available at this time but may be obtained from the authors upon reasonable request.

CRediT authorship contribution statement

Xiaoshuang Wang: Conceptualization, Methodology, Writing –

original draft, Writing – review & editing. **Kun Wang:** Conceptualization, Methodology, Writing – original draft. **Xiaofeng Liu:** Conceptualization, Methodology, Writing – review & editing, Funding acquisition. **Yuan-an Zhao:** Conceptualization, Methodology, Writing – review & editing, Supervision. **Dawei Li:** Validation, Formal analysis. **Zhaoliang Cao:** Funding acquisition, Resources. **Yuchen Shao:** Validation, Formal analysis. **Zenghui Peng:** Funding acquisition, Resources. **Ming Tang:** Funding acquisition, Resources. **Jianda Shao:** Funding acquisition, Resources.

Declaration of competing interest

The authors declare that they have no known competing financial interests or personal relationships that could have appeared to influence the work reported in this paper.

References

[1] T.H. Kim, M. Kim, R. Manda, Y.J. Lim, K.J. Cho, H. Hee, J.-W. Kang, G.-D. Lee, S. H. Lee, Flexible liquid crystal displays using liquid crystal-polymer composite film and colorless polyimide substrate, Curr. Opt. Photon. 3 (2019) 66–71.

[2] X. Zhou, G. Qin, L. Wang, Z. Chen, X. Xu, Y. Dong, A. Moheghi, D.-K. Yang, Full color waveguide liquid crystal display, Opt. Lett. 42 (2017) 3706–3709.

[3] W.-C. Su, W.-B. Hung, H.-Y. Hsiao, Switchable holographic image splitter fabricated with dye-doped liquid crystals, Opt Express 21 (2013) 6640–6649.

[4] J. Li, H.-Y. Tu, W.-C. Yeh, J. Gui, C.-J. Cheng, Holographic three-dimensional display and hologram calculation based on liquid crystal on silicon device [Invited], Appl. Opt. 53 (2014) G222–G231.

[5] A. Bagramyan, L. Tabourin, A. Rastqar, N. Karimi, F. Bretzner, T. Galstian, Focus-tunable microscope for imaging small neuronal processes in freely moving animals, Photon. Res. 9 (2021) 1300–1309.

[6] S. Zhixiong, Z. Shenghang, L. Xinan, G. Shijun, C. Peng, H. Wei, L. Yanqing, Liquid crystal integrated metalens with tunable chromatic aberration, Advanced Photonics 2 (2020), 036002.

[7] X. Chang, X. Tingfa, Y. Ge, M. Xu, Z. Yuhan, W. Xi, Z. Feng, R.A. Gonzalo, Super-resolution compressive spectral imaging via two-tone adaptive coding, Photon. Res. 8 (2020) 395–411.

[8] X. Zhang, Z. Cao, H. Xu, Y. Wang, D. Li, S. Wang, C. Yang, Q. Mu, L. Xuan, High precision system modeling of liquid crystal adaptive optics systems, Opt Express 25 (2017) 9926–9937.

[9] K. Yao, J. Wang, X. Liu, W. Liu, Closed-loop adaptive optics system with a single liquid crystal spatial light modulator, Opt Express 22 (2014) 17216–17226.

[10] J. Heebner, M. Borden, P. Miller, S. Hunter, K. Christensen, M. Scanlan, C. Haynam, P. Wegner, M. Hermann, G. Brunton, E. Tse, A. Awwal, N. Wong, L. Seppala, M. Franks, E. Marley, K. Williams, T. Budge, M. Henesian, J.-M. Dinicola, Programmable beam spatial shaping system for the national ignition facility, Proc. SPIE 7916 (2011) 11.

[11] H. Takahashi, S. Hasegawa, Y. Hayasaki, Holographic femtosecond laser processing using optimal-rotation-angle method with compensation of spatial frequency response of liquid crystal spatial light modulator, Appl. Opt. 46 (2007) 5917–5923.

[12] D. Yufei, L. Feng, Y. Zhi, L. Qianglong, Y. Yang, W. Tianhao, W. Yishan, Y. Xiaojun, Femtosecond chirped pulse amplification system with liquid crystal spatial light modulator for spectral modulation, Chin. J. Lasers 48 (2021) 1101001.

[13] G. Xia, W. Fan, D. Huang, H. Cheng, J. Guo, X. Wang, High damage threshold liquid crystal binary mask for laser beam shaping, High Power Laser Sci. Eng. 7 (2019).

[14] S. Li, Y. Wang, Z. Lu, L. Ding, P. Du, Y. Chen, Z. Zheng, D. Ba, Y. Dong, H. Yuan, Z. Bai, Z. Liu, C. Cui, High-quality near-field beam achieved in a high-power laser based on SLM adaptive beam-shaping system, Opt Express 23 (2015) 681–689.

[15] M. Vieweg, T. Gissibl, S. Pricking, B.T. Kuhlmey, D.C. Wu, B.J. Eggleton, H. Giessen, Ultrafast nonlinear optofluidics in selectively liquid-filled photonic crystal fibers, Opt Express 18 (2010) 25232–25240.

[16] Z. He, K. Yin, S.T. Wu, Miniature planar telescopes for efficient, wide-angle, high-precision beam steering, Light Sci. Appl. 10 (2021) 134.

[17] E. Watson, B. Whitaker, S. Harris, Initial High-Power-CW-Laser Testing of Liquid-Crystal Optical Phased Arrays, 2005, p. 40.

[18] Z. Cao, Q. Mu, L. hu, C. Liu, l. Xuan, The durability of a liquid crystal modulator for use with a high power laser, J. Opt. Pure Appl. Opt. 9 (2007) 427.

[19] G. Zhu, D. Whitehead, W. Perrie, O.J. Allegre, V. Olle, Q. Li, Y. Tang, K. Dawson, Y. Jin, S.P. Edwardson, L. Li, G. Dearden, Investigation of the thermal and optical performance of a spatial light modulator with high average power picosecond laser exposure for materials processing applications, J. Phys. Appl. Phys. 51 (2018), 095603.

[20] T. Xi, J. Di, J. Dou, Y. Li, J. Zhao, Measurement of thermal effect in high-power laser irradiated liquid crystal device using digital holographic interferometry, Appl. Phys. B 125 (2019) 103.

[21] P.Y. Wang, H.J. Zhang, J.H. Dai, Laser-heating-induced self-phase modulation, phase transition, and bistability in nematic liquid crystals, Opt Lett. 13 (1988) 479–481.

[22] V.M. di Pietro, A. Jullien, U. Bortolozzo, N. Forget, S. Residori, Thermally-induced nonlinear spatial shaping of infrared femtosecond pulses in nematic liquid crystals, Laser Phys. Lett. 16 (2018), 015301.

[23] X. Wang, L. Wu, M. Li, S. Wu, J. Shang, Q. Qiu, Theoretical and experimental demonstration on grating lobes of liquid crystal optical phased array, Int. J. Opt. (2016) 1–6, 2016.

[24] G. Vantomme, A.H. Gelebart, D.J. Broer, E.W. Meijer, Self-sustained actuation from heat dissipation in liquid crystal polymer networks, J. Polym. Sci. Polym. Chem. 56 (2018) 1331–1336.

[25] Z. Zhou, X. Wang, R. Zhuo, X. He, L. Wu, X. Wang, Q. Tan, Q. Qiu, Theoretical modeling on the laser-induced phase deformation of liquid crystal optical phased shifter, Appl. Phys. B 124 (2018) 35.

[26] R.J. Carlton, C.D. Ma, J.K. Gupta, N.L. Abbott, Influence of specific anions on the orientational ordering of thermotropic liquid crystals at aqueous interfaces, Langmuir 28 (2012) 12796–12805.

[27] A. Selevou, G. Papamokos, T. Yildirim, H. Duran, M. Steinhart, G. Floudas, Eutectic liquid crystal mixture E7 in nanoporous alumina. Effects of confinement on the thermal and concentration fluctuations, RSC Adv. 9 (2019) 37846–37857.

[28] T. Kim, Chapter 7 - surface heat transfer mapping using thermochromic liquid crystal, in: T. Kim, T.J. Lu, S.J. Song (Eds.), Application of Thermo-Fluidic Measurement Techniques, Butterworth-Heinemann, 2016, pp. 191–214.

[29] S.S. Sastry, T.V. Kumari, C.N. Rao, K. Mallika, S. Lakshminarayana, H.S. Tiong, Transition temperatures of thermotropic liquid crystals from the local binary gray level cooccurrence matrix, Adv. Condens. Matter Phys. (2012) 527065, 2012.

[30] T. Nunak, K. Rakrueangdet, N. Nunak, T. Suesut, Thermal image resolution on angular emissivity measurements using infrared thermography, Lect. Notes Eng. Comput. Sci. 1 (2015) 323–327.

[31] W.J. Zhang, T.M. Wang, L.Z. Zhong, X.W. Wu, M. Cui, Theoretical study of infrared emissivity of indium tin oxide films, Wuli Xuebao/Acta Phys. Sinica 54 (2005) 4439–4444.

[32] L. Chang, G. Cui, Moiré fringe phase difference measurement based on spectrum zoom Technology, TELKOMNIKA Indones. J. Electr. Eng. 11 (2013).

[33] J. Li, S.-T. Wu, Extended Cauchy equations for the refractive indices of liquid crystals, J. Appl. Phys. 95 (2004) 896–901.

[34] J. Li, S. Gauza, S.-T. Wu, Temperature effect on liquid crystal refractive indices, J. Appl. Phys. 96 (2004) 19–24.

[35] J.H. Yoo, M. Matthews, P. Ramsey, A.C. Barrios, A. Carter, A. Lange, J. Bude, S. Elhadj, Thermally ruggedized ITO transparent electrode films for high power optoelectronics, Opt Express 25 (2017) 25533–25545.

[36] J.H. Yoo, M.G. Menor, J.J. Adams, R.N. Raman, J.R. Lee, T.Y. Olson, N. Shen, J. Suh, S.G. Demos, J. Bude, S. Elhadj, Laser damage mechanisms in conductive widegap semiconductor films, Opt Express 24 (2016) 17616–17634.

[37] S. Wolf, D. Studer, K. Wendt, F. Schmidt-Kaler, Efficient and robust photo-ionization loading of beryllium ions, Appl. Phys. B 124 (2018).

[38] Z. Raszewski, W. Piecek, L. Jaroszewicz, L. Soms, J. Marczak, E. Nowinowski-Kruszelnicki, P. Perkowski, J. Kedzierski, E. Miszczyk, M. Olifierczuk, P. Morawiak, R. Mazur, Laser damage resistant nematic liquid crystal cell, J. Appl. Phys. 114 (2013).

[39] V.I. Ustugov, F.L. Vladimirov, N.I. Pletneva, I.E. Morichev, L.N. Soms, V. P. Pokrovskiy, Liquid crystal modulators with improved laser damage resistance, in: Laser Optics, vol. 98, Solid State Lasers, 1998.